Supplementary Information

Boron-Modulated Amorphous Cobalt Layer on Cu Foam Enabling Efficient and Stable Hydrolysis of Ammonia Borane

Kang Wang[#], Shikai Chang[#], Cheng Lu[#], Yufeng Chen, Yong Feng, Youyong Li, Kun Feng and Jun Zhong **

Institute of Functional Nano and Soft Materials Laboratory (FUNSOM), Jiangsu Key Laboratory of Advanced Negative Carbon Technologies, Soochow University, Suzhou 215123, China.

[#] These authors contribute equally to this work.

∗Address correspondence to kunfeng@suda.edu.cn (K. Feng) and jzhong@suda.edu.cn (J. Zhong)

Experimental details

Chemicals and Reagents

All the chemicals were used as received without further purification. $Co(NO_3)_2 \cdot 6H_2O$ (99%), $Ni(NO_3)_2 \cdot 6H_2O$ (99%), $Fe(NO_3)_2 \cdot 9H_2O$ (99%) and sodium borohydride ($NaBH_4$, 98%) were purchased from Sinopharm. Nickel foam, copper foam and zinc foam were purchased from Suzhou Keshenghe Metal Materials Co., Ltd. Ammonia borane (NH_3BH_3, 97%) was purchased from Sigma-Aldrich. De-ionized water was obtained from an ultra-pure purifier (resistivity ≥18.2 MΩ). The fuel cell stack was purchased from Horizon Co., Ltd. This type of fuel cell is a Proton Exchange Membrane (PEM) fuel cell, which requires dry hydrogen with a purity higher than 99.995% for normal operation. All the reagents were analytical grade and used as received without further purification.

Characterization

The samples were measured by high-resolution transmission electron microscope (HRTEM) (FEI Talos F200x). X-ray photoelectron spectrometer (XPS, Thermo Scientific K-Alpha+) and X-ray diffraction (XRD, PANalytical B.V. Empyrean powder diffractometer equipped with PIXcel3D detector) were used for the structure characterization. The metal contents were measured by an inductively coupled plasma spectrometer (ICP-OES, Avio 200). X-ray absorption spectroscopy (XAS) experiments were performed at National Synchrotron Radiation Laboratory (NSRL, MCD-A and MCD-B) and Shanghai Synchrotron Radiation Facility (SSRF, 20U).

Catalytic Activity Measurement

The B-CoCu Foam was put in a one-neck round-bottom flask (25 mL), which was sealed and connected to a gas collecting tube. Then 1 mL AB water solution (3 M) was quickly injected into the flask. The experiment was performed under room temperature and ambient atmosphere. The reaction time was recorded when observing the first bubble. The volume of hydrogen generation was measured

by recording the displacement of water. Produced gas was identified as H_2 using a gas chromatograph. The kinetic isotope effect (KIE) was measured by following the similar reaction procedure, except that D_2O was used to replace H_2O. The hydrolysis process can be described by the formula: $NH_3BH_3 + 2H_2O = NH_4^+ + BO_2^- + 3H_2$. The area catalytic activity (A) is calculated by using the formula: $A=V_{H2}/(S_{Foam}\times t)$, in which V_{H2} is the amount of produced H_2 (mL), S_{Foam} is the macro foam area (cm^2), while t is the reaction time (min).

The TOF value has been calculated by using the surface layer of B-CoCu foam as the active site. The BET value of B-CoCu foam is measured as 4.599 m^2/g, while the weight of the foam is 0.0401 g. The diameter of Co atom is 0.25 nm (0.26 for Cu) and the Co metal density is 8.90×10^6 g/m^3 (8.96×10^6 g/m^3). Thus the amount of three surface layers of B-CoCu foam (both Co and Cu on the surface) is around $4.599\times0.0401\times3\times0.25\times10^{-9}\times8.90\times10^6/58.9=0.0209$ mmol. Then the TOF value can be: $TOF=n_{H2}/(n_{(cat)}\times t)=9/(0.0209\times2.666)=161.5$ (H_2)mol/((Cat-metal)mol·min). For the stability test, 3 mmol AB was injected into the flask again to start the next cycle when the previous cycle was finished.

DFT calculation

All DFT calculations are carried out by using the Vienna ab initio simulation package (VASP). A generalized gradient approximation (GGA) in the form of the Perdew-Burke-Ernzerhof (PBE) functional is applied to account for the electronic exchange-correlation interaction. The projector augmented-wave (PAW) method is adopted to treat the core-valence electron interactions with a cut off energy of 400 eV. The reciprocal space in slab models is described by using a 3 × 3 × 1 k point grid mesh, and Γ point is used for isolated H_2O and NH_3BH_3 molecules. A 2×2×1 supercell is applied for the adsorption calculations, and the convergence tolerances of force and energy for geometric optimization are set as 0.03 $eV/Å^{-1}$ and 1×10^{-5} eV, respectively. The thickness of the vacuum region

is set to over 15 Å along the z-direction (vertical to the surface) to avoid interactions between adjacent layers. The transition states (TS) related to the activation of water and NH_3BH_3 are obtained by combining the climbing-image nudged elastic-band (CI-NEB).

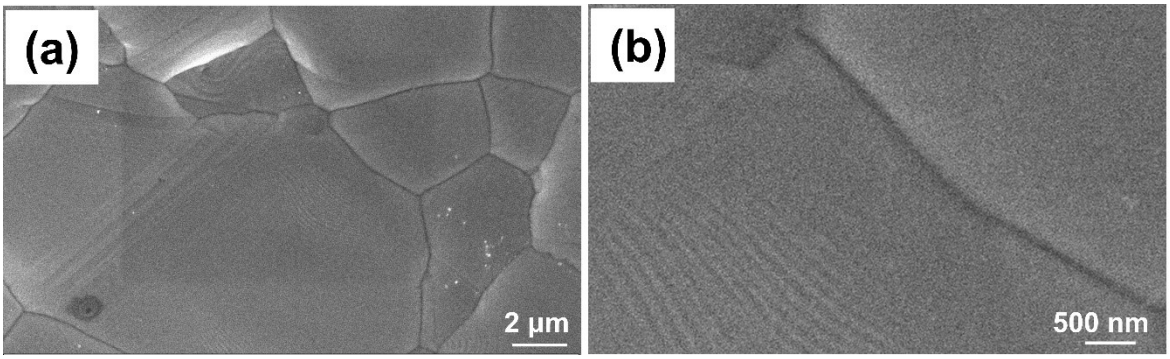

Fig. S1. Low magnification SEM image (a) and high magnification SEM image (b) of Cu foam.

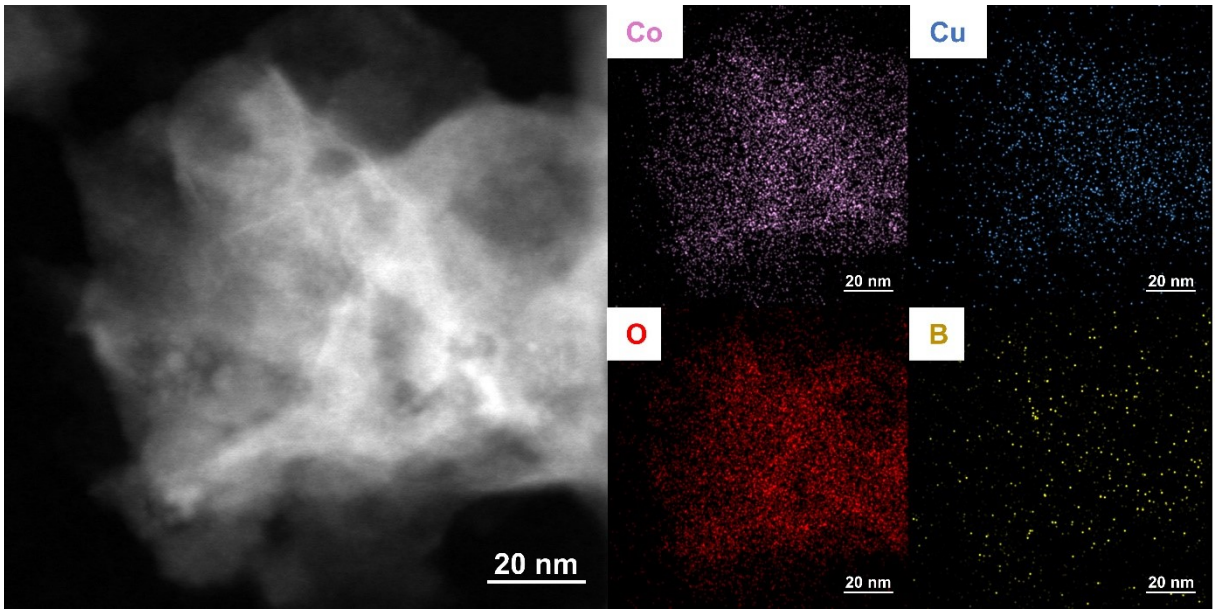

Fig. S2. Dark-field elemental mappings of surface amorphous sheet structure on B-CoCu foam: Co (pink), Cu (blue), O (red), B (yellow).

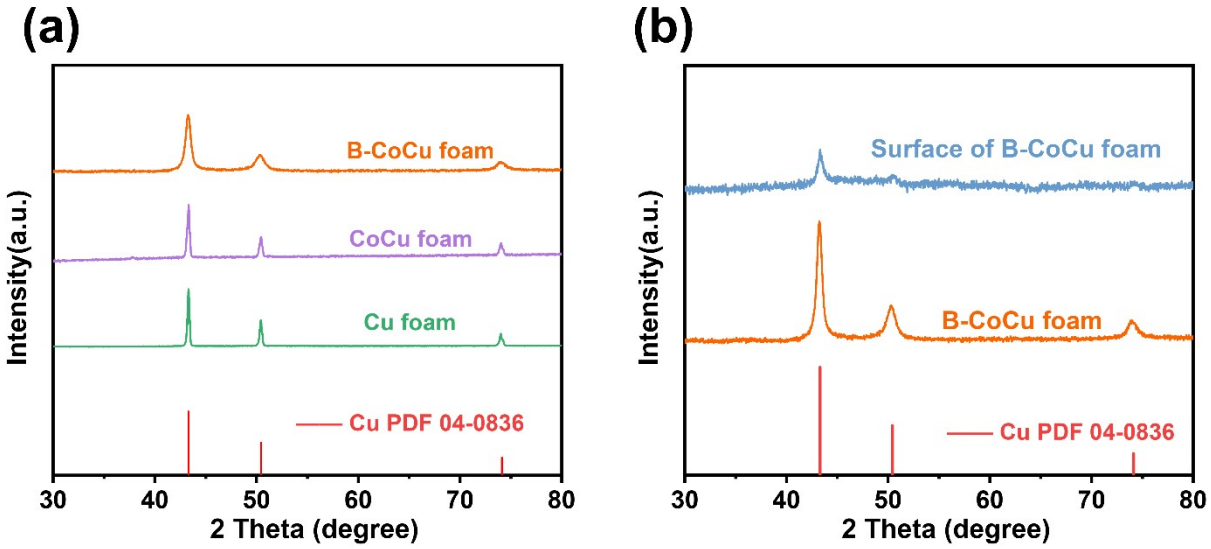

Fig. S3. XRD pattern of (a) B-CoCu foam, CoCu foam, Cu foam and (b) surface of B-CoCu foam (stripped from the surface of B-CoCu foam by ultrasonication).

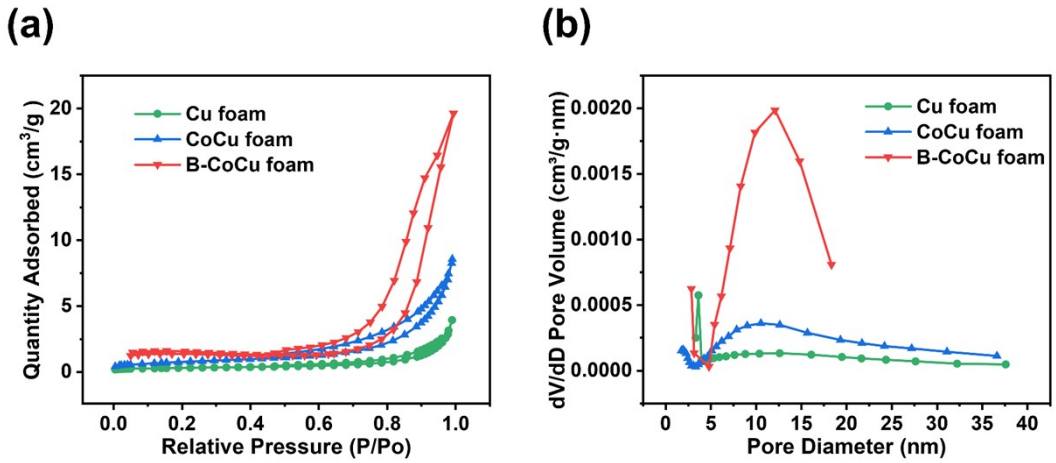

Fig. S4. (a) Nitrogen adsorption/desorption isotherm and (b) the BJH pore-size distribution curves for Cu foam, CoCu foam and B-CoCu foam. The specific surface areas of Cu foam, CoCu foam and B-CoCu foam are 0.933 m^2/g, 2.357 m^2/g and 4.599 m^2/g, respectively. The averaged pore sizes of Cu foam, CoCu foam and B-CoCu foam are 17.93 nm, 12.73 nm and 11.13 nm, respectively.

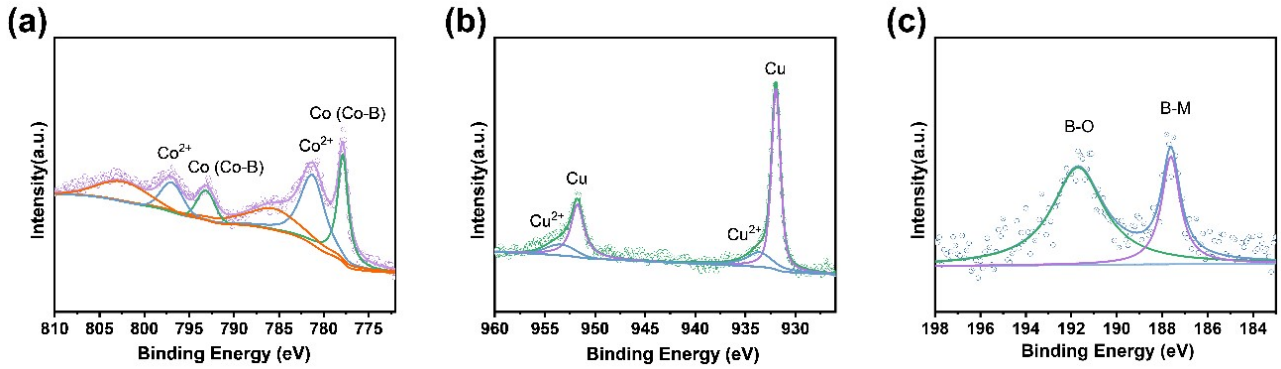

Fig. S5. (a) Co 2p, (b) Cu 2p and (c) B 1s XPS spectra of B-CoCu foam.

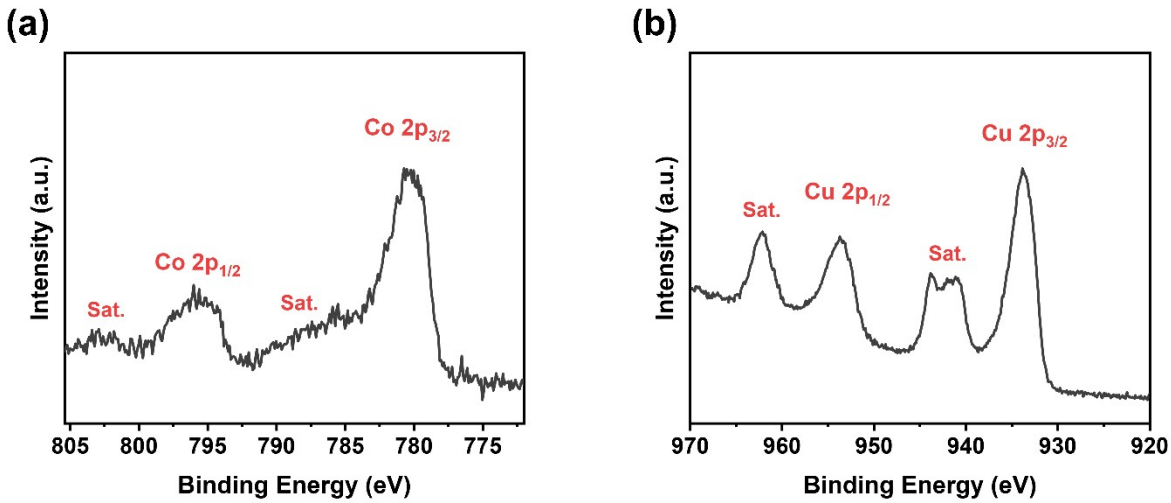

Fig. S6. (a) Co 2p and (b) Cu 2p XPS spectra of CoCuO foam.

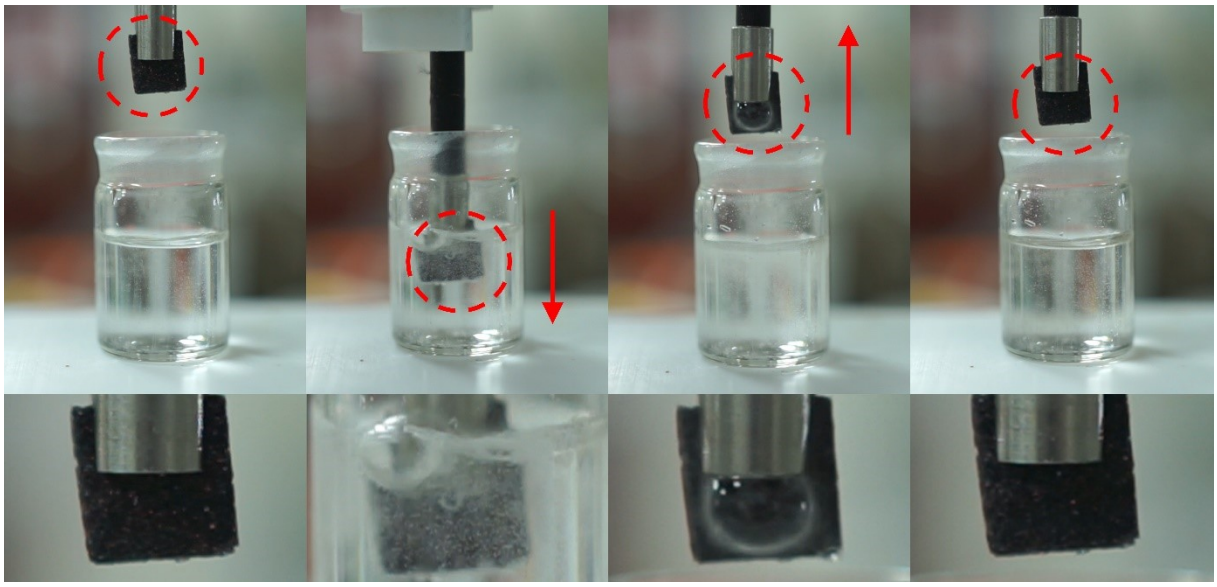

Fig. S7. Hydrolysis images catalyzed by B-CoCu foam.

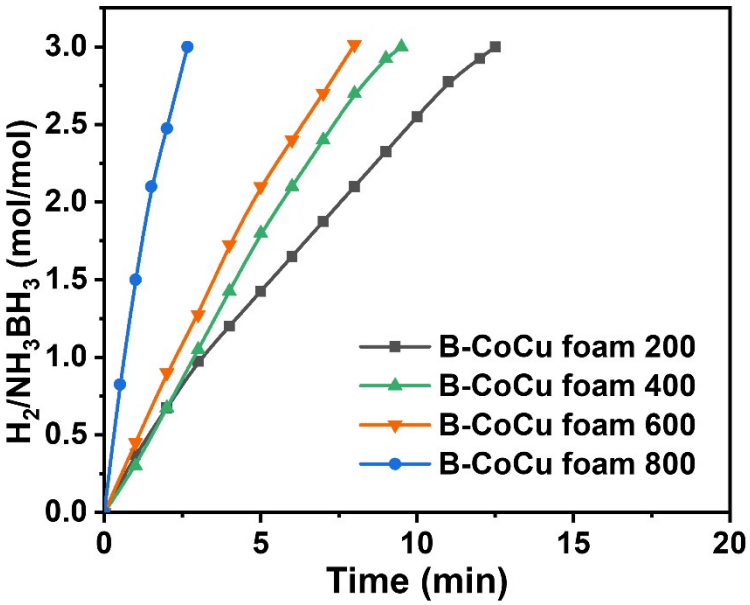

Fig. S8. Hydrogen generation curves of B-CoCu foams treated at different temperatures (200, 400, 600, and 800 °C).

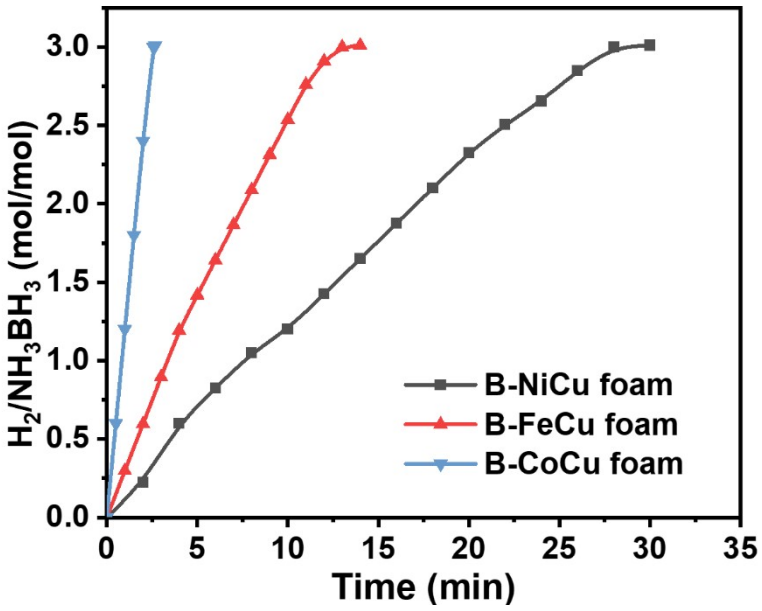

Fig. S9. Hydrogen generation curves by using B-NiCu foam, B-FeCu foam and B-CoCu foam.

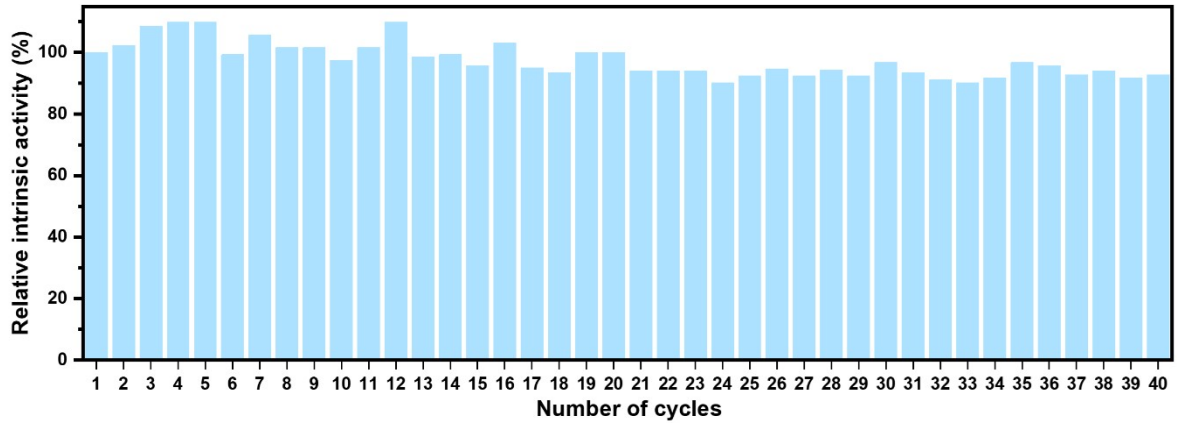

Fig. S10. Relative intrinsic activity of B-CoCu foam subjected to cycling stability tests at 298 K.

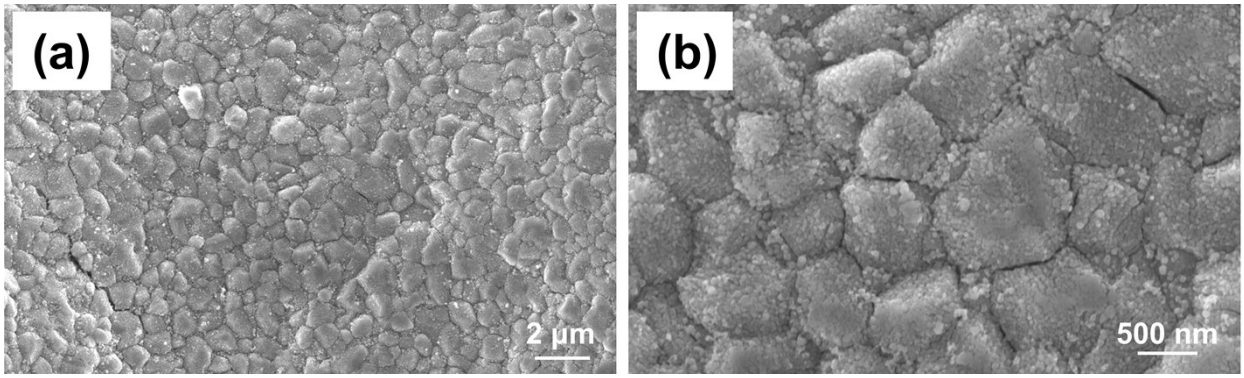

Fig. S11. Low magnification SEM image (a) and high magnification SEM image (b) of B-CoCu foam after working for 40 cycles.

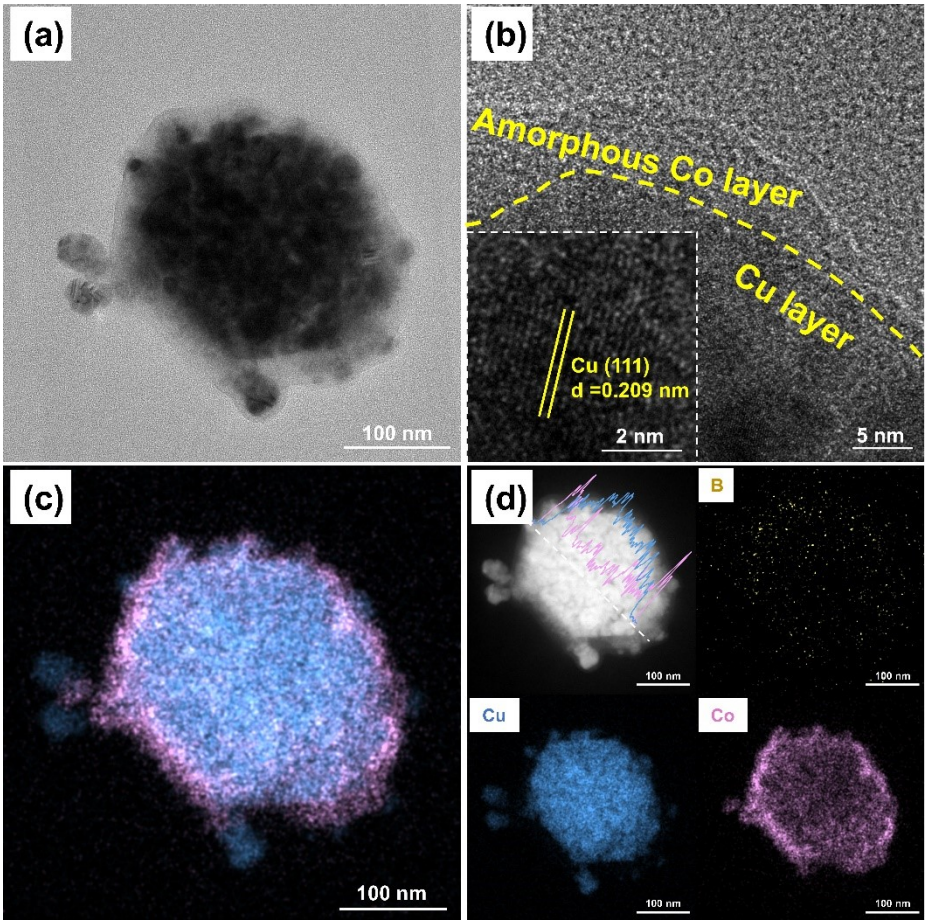

Fig. S12. TEM images with different magnifications (a, b) and EDS-mappings (c, d) of B-CoCu foam after working for 40 cycles.

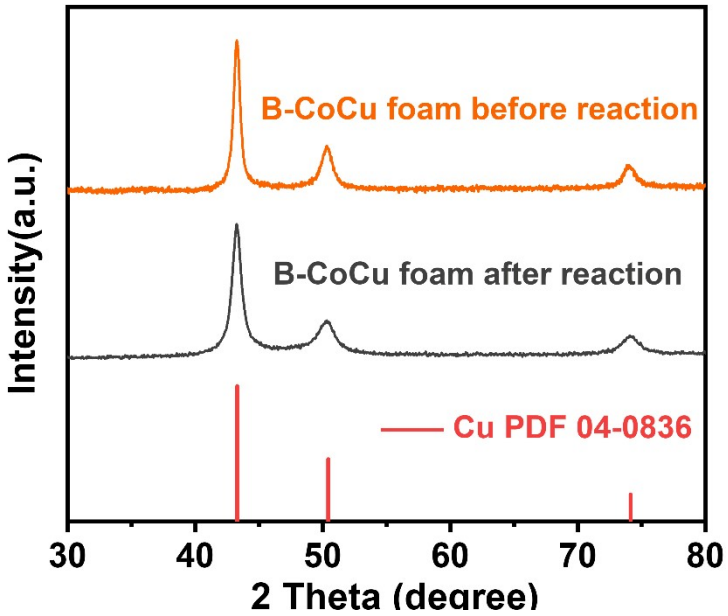

Fig. S13. XRD patterns of B-CoCu foam before reaction and after working for 40 cycles.

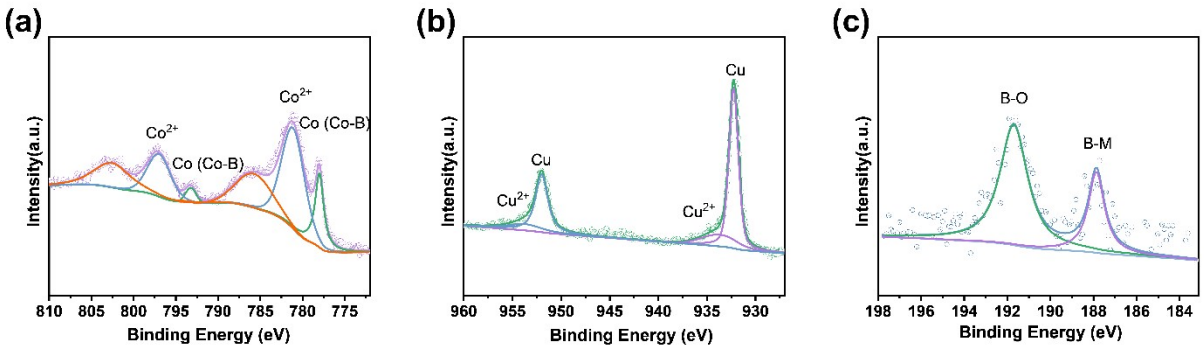

Fig. S14. (a) Co 2p, (b) Cu 2p and (c) B 1s XPS spectra of B-CoCu foam after working for 40 cycles.

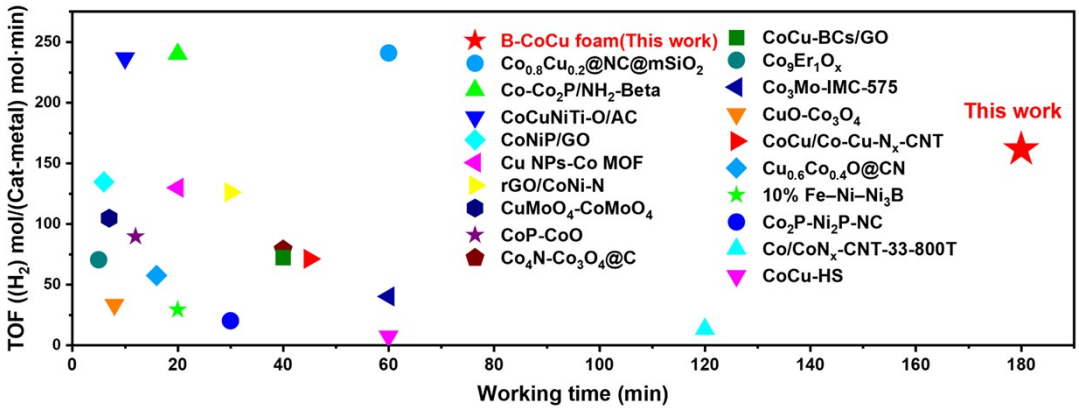

Fig. S15. The comparison of catalytic activity and working time for B-CoCu foam and the reported noble metal-free catalysts.

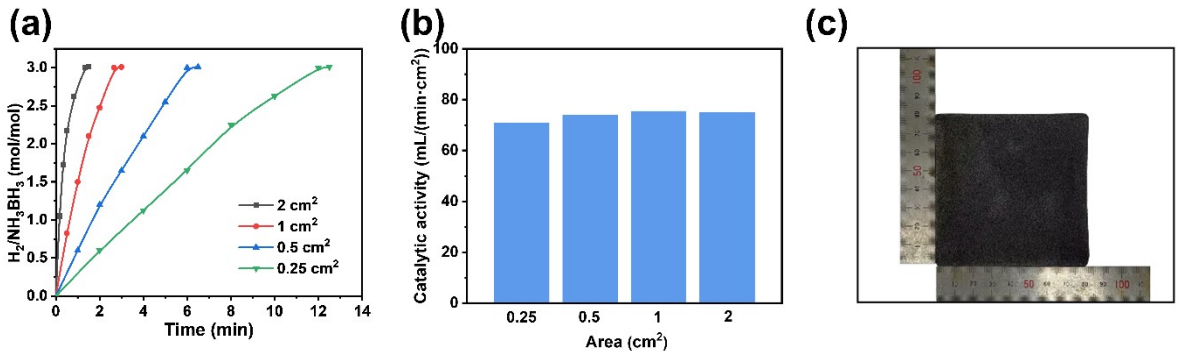

Fig. S16. (a) Hydrogen evolution curves catalyzed by B-CoCu foam with different sizes. (b) Area activities of B-CoCu foam with different sizes. (c) Picture of B-CoCu foam with a size of 8×8 cm^2.

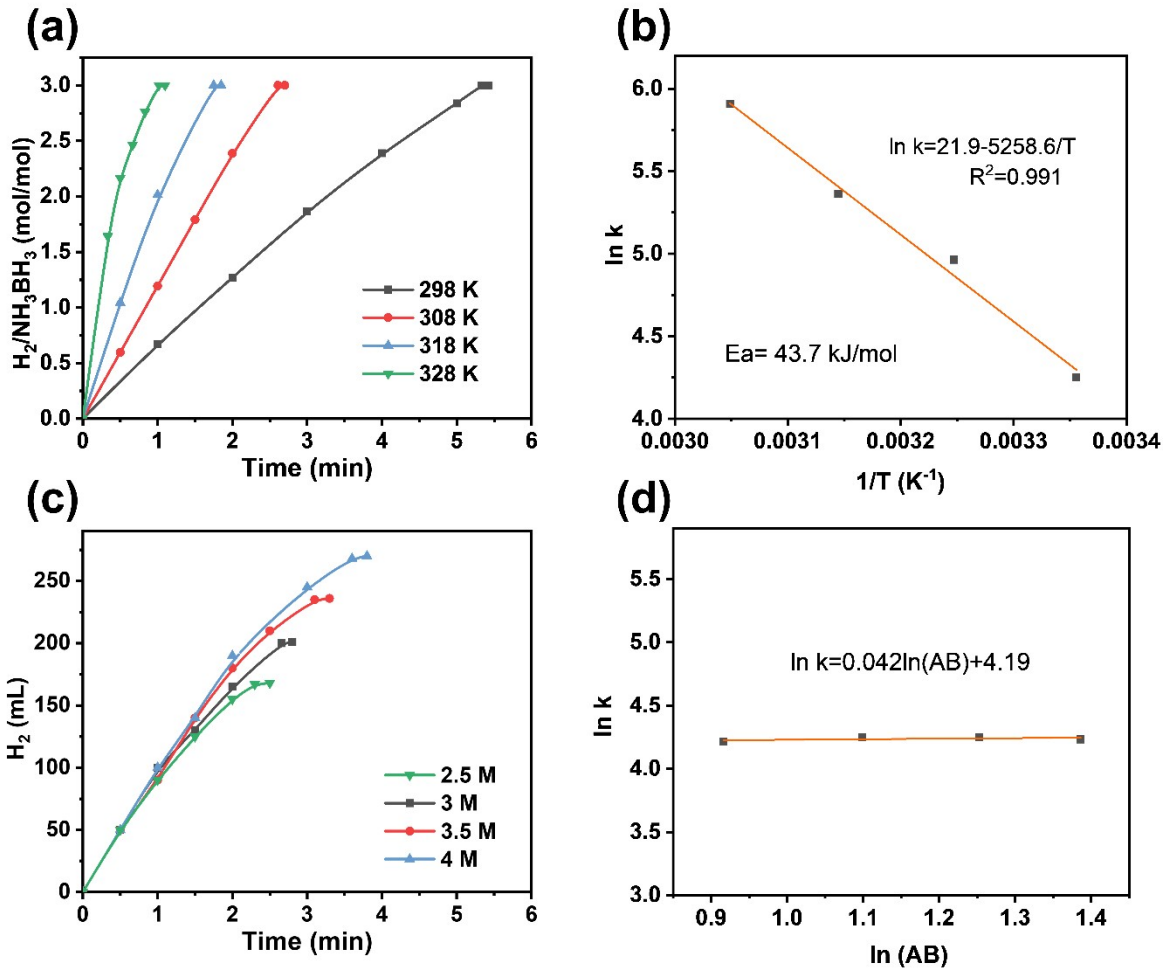

Fig. S17. (a) Hydrogen-generating rate as a function of temperature in the hydrolysis of AB catalyzed by B-CoCu foam and (b) Arrhenius plot of ln k versus 1/T. (c) Relationship between hydrogen-generating rate and AB concentration at a fixed amount of B-CoCu foam and (d) Logarithmic plot of ln k versus AB.

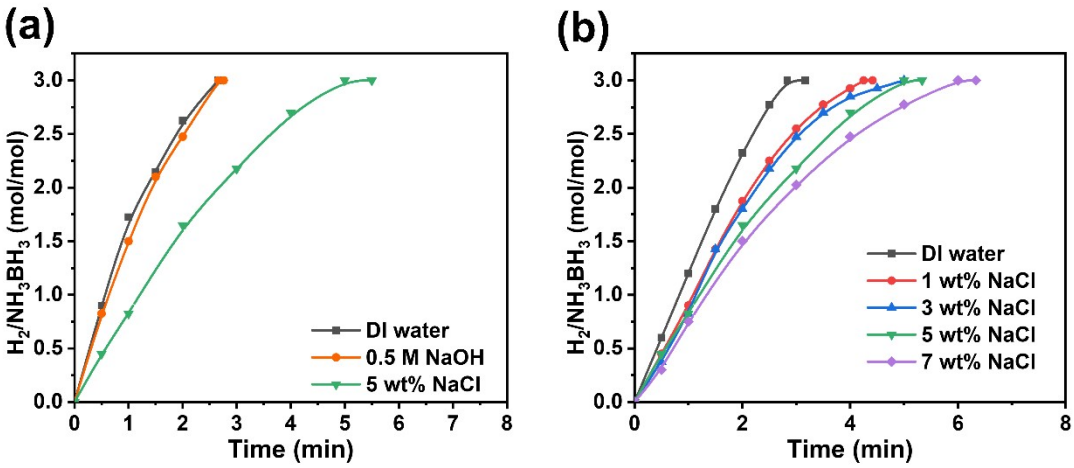

Fig. S18. Hydrogen evolution curves of the hydrolysis of ammonia borane catalyzed by B-CoCu foam in various solutions: (a) DI water, 0.5 M NaOH solution and 5 wt% NaCl solution; (b) NaCl solutions with different concentrations.

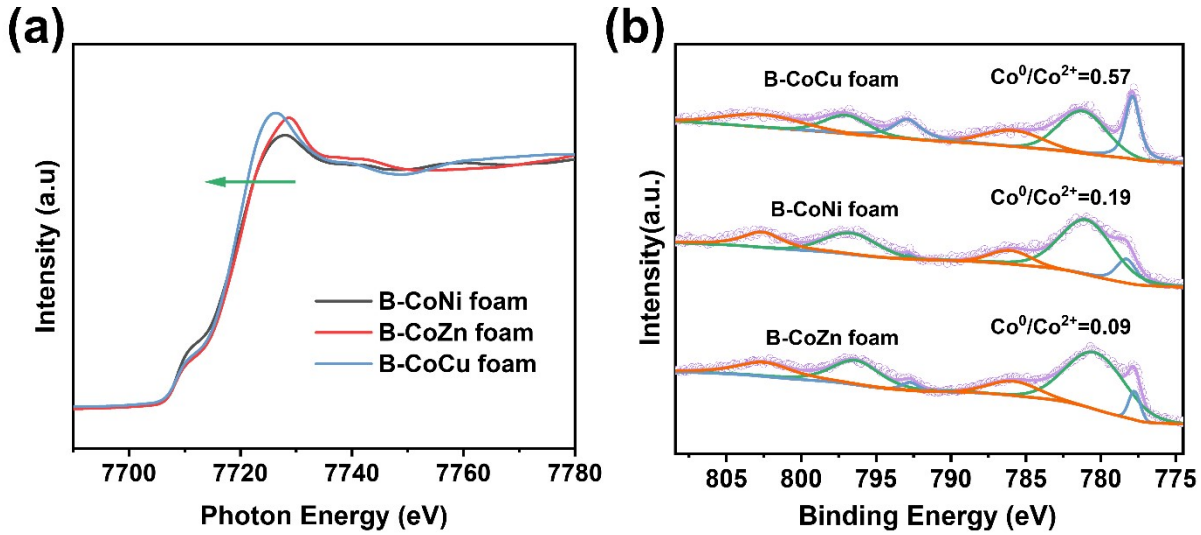

Fig. S19. (a) XANES spectra of B-CoCu foam, B-CoZn foam and B-CoNi foam at Co K-edge. (b) High-resolution XPS spectra of B-CoCu foam, B-CoZn foam and B-CoNi foam at Co 2p.

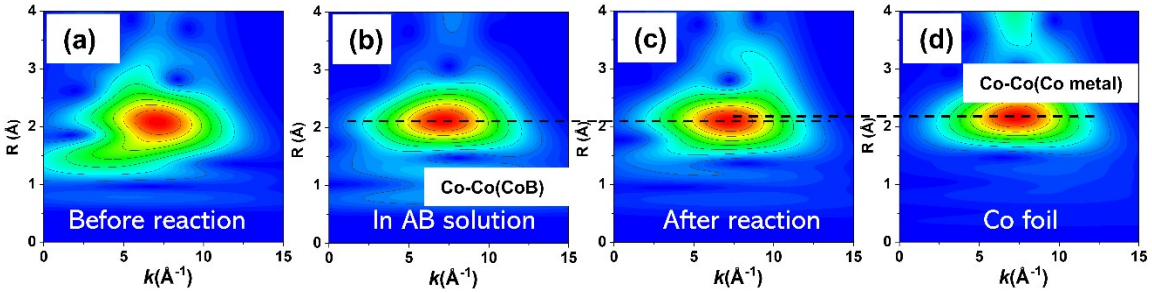

Fig. S20. WT analysis of B-CoCu foam (a) before reaction, (b) in AB solution, (c) after reaction, and (d) Co foil.

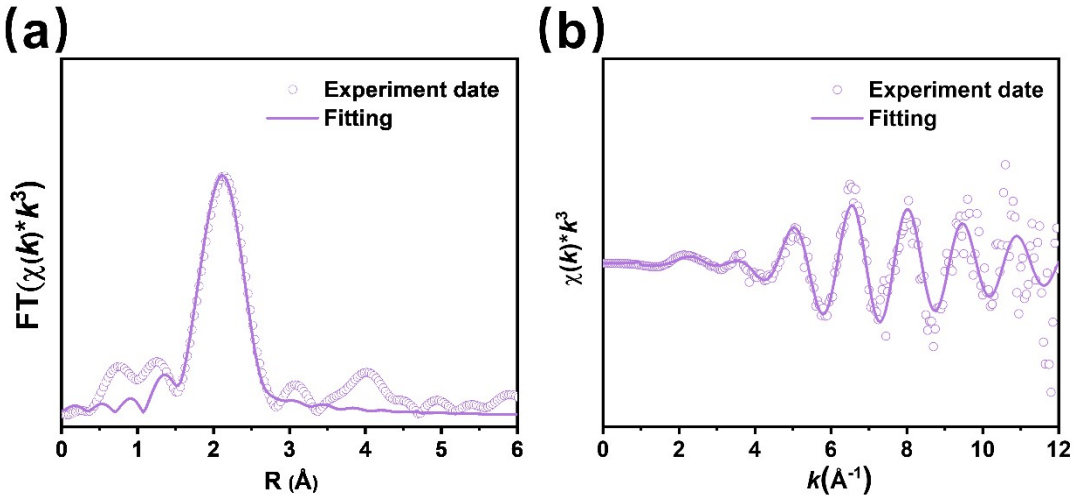

Fig. S21. The EXAFS curve fitting for B-CoCu foam in AB solution at Co K-edge, shown in (a) R-space and (b) *k*-space (k^3 weighted, fitting range: 2-12).

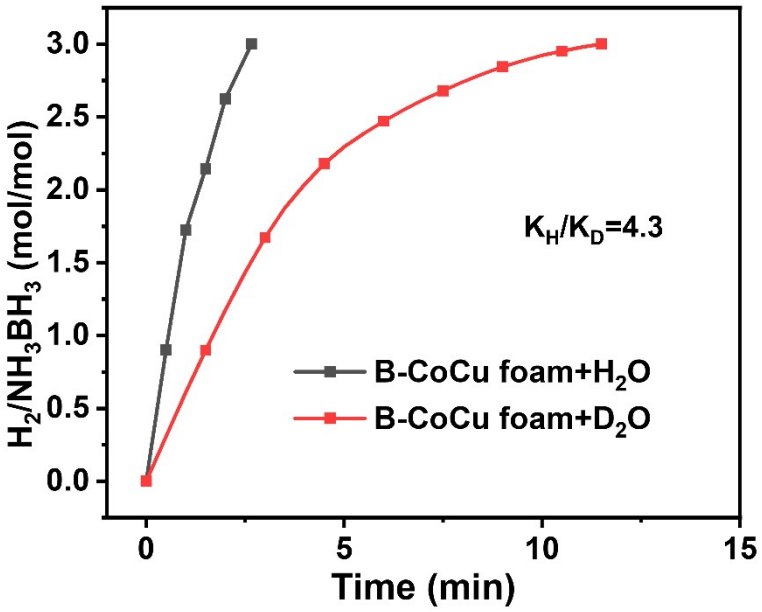

Fig. S22. Hydrogen evolution curves through AB hydrolysis catalyzed by B-CoCu foam with H_2O and D_2O as the reactants at 298 K.

Table S1. The contents of Co, Cu and B in B-CoCu foam (measured by ICP-OES). The residue composition (around 1.3 wt%) might be O element not measured by ICP-OES.

Sample	Co (wt%)	Cu (wt%)	B (wt%)
B-CoCu foam	7.54	90.70	0.44

Table S2. Catalytic performance and stability in this work and reported in the literature.

Sample	TOF (H_2)mol/((Cat-metal)mol·min) (tested in water)	TOF (H_2)mol/((Cat-metal)mol·min) (tested in NaOH solution)	Number of cycles	Working time (min)	T (K)	Ref.
B-CoCu foam	161.5	161.5	40	180	298	This work
$Co_{0.8}Cu_{0.2}$@NC@mSiO_2	240.9	--	30	60	298	1
Ni/P-Mo@Mo_2C	222.0	--	10	20	298	2
Co_2P-CDs/mHNTs	178.0	--	6	25	298	3
Ni/$Ti_3C_2T_x$-4	161.0	--	9	20	298	4
rGO/CoNi-N	126.0	--	10	30	298	5
Co_4N-Co_3O_4@C	79.0	--	10	40	298	6
CoCu/Co-Cu-N_x-CNT	71.2	--	30	45	298	7
$Co_9Er_1O_x$	70.5	--	5	5	298	8
CoP/Co_2Ps	64.1	--	10	11	298	9
$Cu_{0.6}Co_{0.4}$O@CN	57.5	--	6	16	298	10
10% Fe–Ni–Ni_3B	29.3	--	12	20	298	11
Co_2P-Ni_2P-NC	20.2	--	5	30	298	12
Co/CoNx-CNT-33-800T	13.3	--	40	120	313	13
Co-Co_2P/NH_2-Beta	--	240.0	10	20	298	14
CoCuNiTi-O/AC	--	236.6	6	10	298	15
CoNiP/GO	--	134.6	5	6	298	16
Cu NPs-Co MOF	--	129.8	10	20	298	17
$CuMoO_4$-$CoMoO_4$	--	104.7	5	7	298	18
CoO_{10}-Cu_2O_1@NC	--	97.0	5	7	298	19
CoP-CoO	--	89.6	5	12	298	20
CoCu-BCs/GO	--	72.4	5	40	298	21
Co_3Mo-IMC-575	--	40.2	5	60	298	22
NiCo-NC	--	35.2	6	8	298	23

$CuO\text{-}Co_3O_4$	--	33.4	5	8	298	24
$Co@Co_2Mo_3O_8$	--	17.3	6	20	298	25
CoCu-HS	--	7.4	10	60	298	26

Table S3. Fitting parameters for the EXAFS data of B-CoCu foam in AB solution and Co foil at Co K-edge.

Sample	Path	S_0^2	CN	R (Å)	ΔE (eV)	σ^2(Å^2)
B-CoCu foam in AB	Co-Co	0.76	5.13	2.47	4.15	0.0080
	Co-B	0.76	1.49	2.11	4.15	0.0066
Co foil	Co-Co	0.76	12	2.49	7.93	0.0061

References

1. C. Wan; R. Li; J. Wang; D. g. Cheng; F. Chen; L. Xu; M. Gao; Y. Kang; M. Eguchi and Y. Yamauchi, *Angew. Chem. Int. Ed.*, 2024, **63**, e202404505.
2. Q. Yao; F. Zhu; J. Long; J. Huo; M. Huang and Z.-H. Lu, *Chem. Eng. J.*, 2025, **520**, 166442.
3. Y. Zhao; S. Guo; X. Xue; C. Xiong; X. Gao and B. Zhang, *Chem. Eng. J.*, 2024, **483**, 149332.
4. B. Mo; S. Li; H. Wen; H. Zhang; H. Zhang; J. Wu; B. Li and H. Hou, *ACS Appl. Mater. Interfaces*, 2022, **14**, 16320-16329.
5. P. Li; R. Chen; S. Zhao; W. Li; Y. Lin and Y. Yu, *Appl. Catal. B:Environ.*, 2021, **298**, 120523.
6. S. Guan; Y. Liu; H. Zhang; H. Wei; T. Liu; X. Wu; H. Wen; R. Shen; S. Mehdi; X. Ge; C. Wang; B. Liu; E. Liang; Y. Fan and B. Li, *Small*, 2022, **18**, e2107417.
7. D. W. S. Suen, C. Y. V. Li, X. Y. Sun, J. J. Chen, C. Z. Yang, M. Qiu, X. Y. Lu, B. Wang, S. Y. Niu, W. Liu and C. W. Tsang, *J. Colloid Interface Sci.*, 2025, **700**, 138560.
8. K. Wang; Y. Chen; S. Li; K. Feng; S. Wang and J. Zhong, *ACS Materials Lett.*, 2023, **5**, 1188-1195.
9. C. Wan; X. Liu; J. Wang; F. Chen and D. G. Cheng, *Nano Res.*, 2023, **16**, 6260-6269.
10. W. J. Xu, S. L. Zhang, R. F. Shen, Z. K. Peng, B. Z. Liu, J. Li, Z. Y. Zhang and B. J. Li, *Energy Environ. Mater.*, 2023, **6**, e12279.
11. R. K. Borah, A. P. Fatrekar, P. Bakre, S. G. Tilve and A. A. Vernekar, *J. Mater. Chem. A*, 2022, **10**, 25490-25499.
12. S. Mehdi, S. L. Liu, Y. Y. Liu, H. J. Wei, S. Ashraf, R. F. Shen, H. H. Zhang, X. J. Guo, X. L. Wu, T. Liu, J. C. Jiang, Y. F. Wang and B. J. Li, *Small*, 2025, **21**, 2500188.
13. P. C. Poon, Y. H. Wang, W. Q. Li, D. W. S. Suen, W. W. Y. Lam, D. Z. J. Yap, B. L. Mehdi, J. Qi, X. Y. Lu, E. Y. C. Wong, C. Z. Yang and C. W. Tsang, *J. Mater. Chem. A*, 2022, **10**, 5580-5592.
14. S. Wang; Y. Yu; T. Jiang; T. Zhang; Y. Li and Q. Sun, *Small*, 2025, **21**, e2506106.
15. N. Lei; P. Zhou; J. Zhang; F. Chu; C. Cheng; L. Chen; L. Ouyang and X. Xiao, *J. Energy Chem.*, 2025, **110**, 920-931.
16. Y. F. Chen; K. Feng; G. T. Yuan; Z. H. Kang and J. Zhong, *Chem. Eng. J.*, 2022, **428**, 131219.

17. W. Xu; W. Li; H. Wen; J. Ding; Y. Liu; W. Li and B. Li, *Appl. Catal. B:Environ.*, 2021, **286**, 119946.
18. Y. Feng, Y. Shao, X. Chen, Y. Zhang, Q. Liu, M. He and H. Li, *ACS Appl. Energ. Mater.*, 2021, **4**, 633-642.
19. J. R. Zhang; Y. Q. Jia; F. Chu; N. Lei; J. P. Bi; H. Y. Qin; M. L. Liu; Y. X. Jia; L. Zhang; L. Jiang; L. Z. Ouyang and X. Z. Xiao, *Rare Metals*, 2025, **44**, 5486-5497.
20. H. Wu; Y. Cheng; B. Wang; Y. Wang; M. Wu; W. Li; B. Liu and S. Lu, *J. Energy Chem.*, 2021, **57**, 198-205.
21. Y. F. Chen; K. Wang; K. Q. Nie; J. O. Wang; S. F. Wang; K. Feng and J. Zhong, *Chem. Eng. J.*, 2023, **451**, 138931.
22. J. He; P. Zhou; X. Xiao; F. Chu; L. Ouyang; B. Liu; R. Li; Z. Huang; L. Hu; S. Yuan; T. Zhou; X. Fan and L. Chen, *Chem. Eng. J.*, 2023, **474**, 145604.
23. L. Zhao; Q. Wei; L. Zhang; Y. Zhao and B. Zhang, *Renew. Energ.*, 2021, **173**, 273-282.
24. J. Liao; Y. Feng; X. Zhang; L. Huang; S. Huang; M. Liu; Q. Liu and H. Li, *ACS Appl. Nano Mater.*, 2021, **4**, 7640-7649.
25. J. He; Z. Huang; W. Chen; X. Xiao; Z. Yao; Z. Liang; L. Zhan; L. Lv; J. Qi; X. Fan and L. Chen, *Chem. Eng. J.*, 2022, **431**, 133697.
26. L. Liu, Z. J. Zhou, Y. Liu, X. Yu, D. X. Yu and M. H. Xu, *J. Mater. Chem. A*, 2026, **14**, 4628-4639.